



HAL
open science

Measurement of dispersion curves of circumferential guided waves radiating from curved shells: Theory and numerical validation

Mathieu Chekroun, Jean-Gabriel Minonzio, Claire Prada, Pascal Laugier,
Quentin Grimal

► To cite this version:

Mathieu Chekroun, Jean-Gabriel Minonzio, Claire Prada, Pascal Laugier, Quentin Grimal. Measurement of dispersion curves of circumferential guided waves radiating from curved shells: Theory and numerical validation. *Journal of the Acoustical Society of America*, 2016, 139 (2), pp.790. 10.1121/1.4941652 . hal-01305025

HAL Id: hal-01305025

<https://hal.sorbonne-universite.fr/hal-01305025v1>

Submitted on 20 Apr 2016

HAL is a multi-disciplinary open access archive for the deposit and dissemination of scientific research documents, whether they are published or not. The documents may come from teaching and research institutions in France or abroad, or from public or private research centers.

L'archive ouverte pluridisciplinaire **HAL**, est destinée au dépôt et à la diffusion de documents scientifiques de niveau recherche, publiés ou non, émanant des établissements d'enseignement et de recherche français ou étrangers, des laboratoires publics ou privés.

**Measurement of dispersion curves of
circumferential guided waves radiating from curved shells:
Theory and numerical validation**

Running Title : **Circumferential guided waves on curved shells**

March 23, 2015

Mathieu Chekroun¹

Laboratoire d'Acoustique de l'Université du Maine UMR-CNRS 6613,
av. Olivier Messiaen, 72085 Le Mans cedex 9, France

Jean-Gabriel Minonzio

Sorbonne Universités, UPMC Univ Paris 06, CNRS UMR 7371,
INSERM UMR_S 1146, Laboratoire d'Imagerie Biomédicale, F-75005, Paris, France

Claire Prada

Institut Langevin, Ecole Supérieure de Physique et de Chimie Industrielles Paris Tech,
Université Denis Diderot Paris 7, CNRS 7587, 1 rue Jussieu, F-75005 Paris, France

Pascal Laugier and Quentin Grimal

Sorbonne Universités, UPMC Univ Paris 06, CNRS UMR 7371,
INSERM UMR_S 1146, Laboratoire d'Imagerie Biomédicale, F-75005, Paris, France

¹Author to whom correspondence should be addressed. Electronic mail: mathieu.chekroun@univ-lemans.fr

Abstract

A method is proposed to evaluate in a non-contact way the phase velocity dispersion curves of circumferential waves around a shell of arbitrary shape immersed in a fluid. No assumptions are made about the thickness nor the material of the shell. A geometrical model is derived to describe the shape of the radiated wavefronts in the surrounding fluid, and predict the positions of its centers of curvature. Then the time-reversal principle is applied to recover these positions and to calculate the phase velocity of the circumferential waves. Numerical finite-difference simulations are performed to evaluate the method on a circular and on an elliptic thin shells. The different dispersion curves branches can be recovered with an error of less than 10%.

PACS numbers : 43.20.Mv, 43.30.Jx, 43.40.Rj

1 I INTRODUCTION

2 Circumferential waves are interface-type waves propagating around a cylindrical object.
3 They can be classified into two groups : internal and external waves. The external waves
4 (generalized Stoneley waves, Franz waves, creeping waves) reside essentially at the external
5 interface of the object. Their velocity is close to that of the waves in the surrounding medium
6 (water in the present case). The internal waves are analogous to Rayleigh waves in the case
7 of a plain cylinder or to Lamb waves in the case of shells. They depend on the material
8 constituting the scatterer, and are thus suitable to perform evaluation or characterization of
9 the material.

10 Circumferential waves are generated when an incident wave hits the interface at a critical
11 angle of incidence β where, following Snell's law, $\beta = \text{asin} \frac{c_0}{c_\phi}$, c_0 and c_ϕ denoting the phase
12 velocities of acoustic waves in the surrounding medium and of the circumferential wave, re-
13 spectively. During the propagation, circumferential waves radiate in the surrounding medium
14 at the same angle β , and thus contribute to the scattered field when a revolution object is hit
15 by an incident wave. This can be underlined for example by applying a Sommerfeld-Watson
16 transform on the classical partial wave decomposition of the scattered field : the contri-
17 butions may be separated into geometrical components (specular reflection, transmission)
18 and circumferential waves [1, 2, 3]. At high frequencies, the contribution of the radiated
19 circumferential waves in a given point may be evaluated using the Geometrical Theory of
20 Diffraction [4], which has especially been applied on spheres [5].

21 Visualization of the radiated waves can be done using the Schlieren method, allowing
22 the observation of the wavefronts shape [6, 7, 8]. The geometrical shape of these wavefronts
23 have been studied in [6, 9, 10]. In particular, in the case of a circular cylinder of radius
24 a , the wave front equation have been shown to be an involute of a circle of radius $(a \sin \beta)$
25 with the same center as the cylinder [11]. Figure 1 (adapted from [6]) shows the geometrical
26 construction of the radiated wavefronts.

27 The aim of this paper is to describe a method to evaluate the dispersion curves of cir-
28 cumferential guided waves in thin shells of arbitrary geometry immersed in a fluid, observed
29 at a distance by an array of receivers. The method was initially suggested by Thomas et

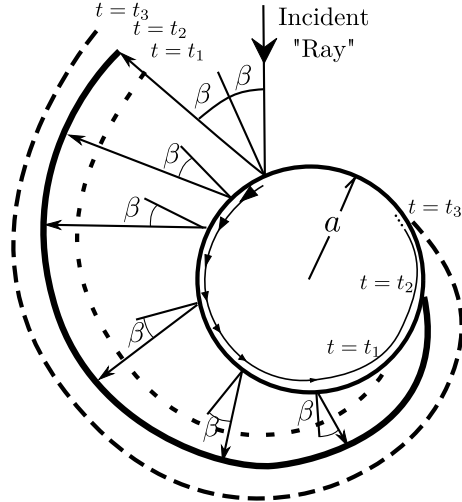


Figure 1: Geometrical construction of the radiated wavefront by a circumferential wave around a circular cylinder (adapted from ref. [6]).

30 al. [12] for thin circular cylindrical shells, based on the time reversal of the waves radiated
 31 in the fluid by the circumferential waves. Building on the later, Prada al. [13] were able to
 32 measure several lamb modes dispersion branch by applying the DORT method (a French
 33 acronym for *Décomposition de l'Opérateur de Retournement Temporel*), taking advantages
 34 of the analysis of the iterative time reversal operators [14]. In particular, the DORT method
 35 allowing the separation of the different contributions in the case of multi-modal propagation
 36 of the circumferential waves. Experimental application was successfully conducted on a thin
 37 cylindrical steel shell [12, 13] and on a thicker cylindrical bone mimicking phantom [15, 16].
 38 The later work on a bone mimicking phantom was motivated by the potential to measure the
 39 properties of the cortical shell of the femoral neck by an ultrasound scanner, in the context
 40 of osteoporosis fracture risk assessment. In order to accommodate the complex geometry of
 41 the femoral neck, the method of measurement of circumferential waves was first extended
 42 from circular shell to a particular case of elliptic shells where the major axis of the ellipse
 43 is parallel to the transducer array [17]. In the present paper, the basis of the method is
 44 revisited and a generalization is proposed to evaluate cylindrical objects, the external cross
 45 section of which can be circular as in [12, 13, 15], elliptic, or of arbitrary geometry.

46 II CONFIGURATIONS

47 The method introduced in this article processes the wavefront radiated in an acoustic medium
 48 by a circumferential wave to recover its phase velocity. It can in principle be applied to any
 49 cylindrical shell of arbitrary cross section. For the purpose of illustration the details of the
 50 configurations given below will be used throughout the remaining of the article.

51 Three different cylindrical shells will be considered

- 52 • A circular shell of radius $a=10$ mm;
- 53 • An elliptical shell of major semi-axis $r_1=10$ mm and minor semi-axis $r_2=7.5$ mm, with
 54 the major axis oriented parallel to the array ($\alpha = 0^\circ$);
- 55 • The same elliptical shell, but with its major axis oriented at an angle $\alpha = 30^\circ$.

56 In the case of the ellipses, α denotes the angle between the major axis and an axis parallel
 57 to the array. For all the cases, the thickness of the shell is constant and taken to $e=1$ mm.
 58 With the typical mean radius of the shell $a=10$ mm, the ratio e/a is small (weak curvature
 59 of the shell). As a consequence, the properties of the circumferential guided modes will be
 60 close to those of the leaky Lamb modes in a plane plate [18, 19, 20]. With the frequency
 61 range of interest centered around $f_0=1$ MHz ($ke \simeq 4$ in water), three Lamb modes will be
 62 observed. The external fluid surrounding the shell is water, and the shell is considered as
 63 filled with air. The chosen properties of the medium constituting the shell are close to those
 64 of the cortical bone [21] (table 1).

Table 1: Material properties used for simulations (Longitudinal velocity c_L , shear velocity c_T and density ρ)

	c_L	c_T	ρ
	(m.s ⁻¹)	(m.s ⁻¹)	(g.cm ⁻³)
Water	1500	-	1
Shell	4000	1800	1,85

65 A 128 elements transducer array of total width $D=64$ mm is used to record the radiated
 66 wavefronts in order to determine the phase velocity c_φ by applying the time reversal principle.

67 This transducer is located at a distance $F=60$ mm from the center of the object. The general
 68 configuration for the simulations is presented in fig. 2.

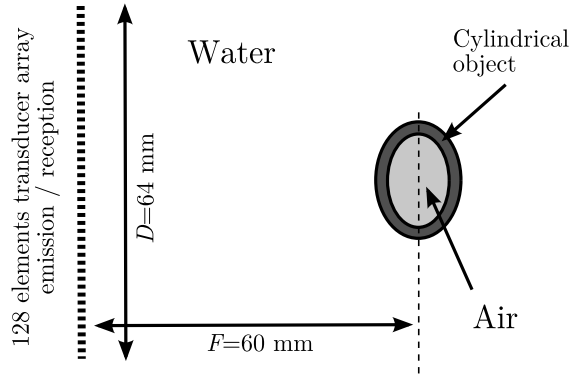


Figure 2: General configuration of the setup used to evaluate the dispersion curves of the circumferential guided waves around a thin cylindrical shell.

68

69 III CASE OF CIRCUMFERENTIAL WAVES IN ELLIPTICAL SHELLS OB- 70 SERVED AT A VERY LARGE DISTANCE

71 At a distance of the shell, the radiated rays seem to arise from a virtual point source inside
 72 the object [22]. The position of this virtual source depends on both the phase velocity of the
 73 circumferential wave (through the critical angle β) and the geometrical shape of the shell. By
 74 applying the time reversal principle [23] it is possible to retrieve the position of this virtual
 75 source as a focal spot. The position of the latter is then used to recover the phase velocity
 76 c_φ for each frequency [12]. In the case of a circular shell, the incident plane wave generates
 77 a pair of symmetrical circumferential waves traveling in opposite directions (clockwise and
 78 counterclockwise), providing two distinct virtual sources (see fig. 3). If the assumption is
 79 made that the receivers are located toward the infinity in the left, the distance d between
 80 these virtual sources is linked with the phase velocity c_φ with the relation

$$c_\varphi = \frac{2ac_0}{d}, \quad (1)$$

81 c_0 denoting the celerity in the surrounding fluid and a the external radius of the cylinder.

82 The same argument as in [12] has been applied to the case of an elliptic shell with major
 83 semi-axis r_1 and minor semi-axis r_2 , and which major axis is parallel to the transducer

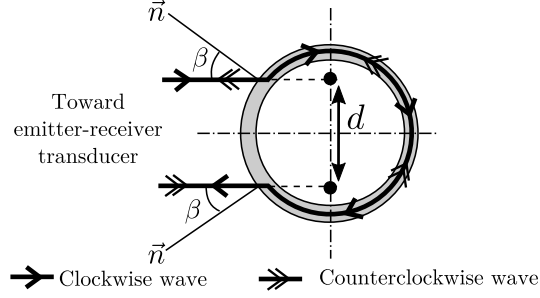


Figure 3: Principle of the generation and radiation of circumferential waves around a thin circular cylinder.

84 array [17]. This leads to the explicit relation (2)

$$c_\varphi = \frac{c_0}{r_2 d} \sqrt{4r_1^4 + (r_2^2 - r_1^2)d^2}, \quad (2)$$

85 linking the dimensions of the ellipse r_1 , r_2 , the celerity c_0 in the surrounding fluid, and the
 86 distance d between the two focal spots obtained by time reversal. In particular, the result
 87 of eq.(1) for the circular shell is retrieved when putting $r_1 = r_2 = a$ in eq (2).

88 In the case of an elliptic shell with an arbitrary orientation compared to the array, or in
 89 the case of a shell of arbitrary cross section, the derivation of a relation such as eq. (2) is
 90 much more complex. In particular, the symmetry with respect to the horizontal axis is lost,
 91 which imposes the upper and lower parts of the shell to be considered separately. Moreover
 92 in equations (1) or (2), the assumption is made that the transducer array is located at an
 93 infinite distance, so that the radiation of the circumferential wave is considered to be parallel
 94 to the horizontal axis, which is obviously not the case, in particular for the receivers located
 95 at the edges of the array. These limitations are addressed in the rest of the paper.

96 IV GEOMETRICAL MODEL OF THE RADIATED WAVEFRONT

97 In this section we develop a model to describe the radiation of circumferential guided waves
 98 using geometrical acoustics.

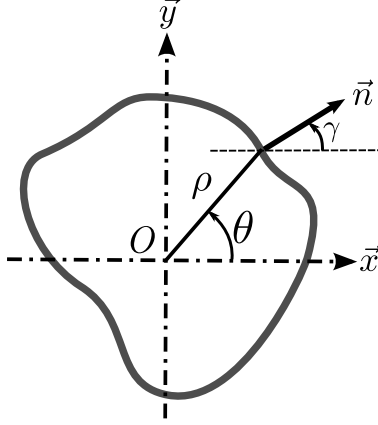


Figure 4: Notations used to describe the radiation of a circumferential wave around a shell of arbitrary cross section.

99 A Description of the shell

100 We consider a thin cylindrical shell of arbitrary cross section, the edge of which is described
 101 by the polar curve $\rho(\theta)$ (see fig. 4). It corresponds to the Cartesian coordinates

$$\begin{cases} x(\theta) = \rho(\theta) \cos \theta \\ y(\theta) = \rho(\theta) \sin \theta \end{cases} \quad (3)$$

102 The external normal vector \vec{n} for each point of the shell is defined by the relation

$$\vec{n}(\theta) = \begin{cases} n_x = \frac{y'}{\sqrt{y'^2 + x'^2}} = \frac{\rho' \sin \theta + \rho \cos \theta}{\sqrt{\rho'^2 + \rho^2}} \\ n_y = \frac{-x'}{\sqrt{y'^2 + x'^2}} = \frac{\rho \sin \theta - \rho' \cos \theta}{\sqrt{\rho'^2 + \rho^2}} \end{cases} \quad (4)$$

103 where the $'$ denotes the derivative with respect to θ . \vec{n} can also be defined by its orientation
 104 γ relative to the horizontal axis \vec{x} (see Fig. 5), expressed as

$$\tan \gamma(\theta) = \frac{n_y}{n_x} = \frac{\rho \sin \theta - \rho' \cos \theta}{\rho' \sin \theta + \rho \cos \theta}. \quad (5)$$

105 Finally, the arc length $s(\theta_1, \theta_2)$ between two points of the shell defined by the polar angles
 106 θ_1 and θ_2 is

$$s(\theta_1, \theta_2) = \int_{\theta_1}^{\theta_2} \sqrt{\rho'(\theta)^2 + \rho(\theta)^2} d\theta. \quad (6)$$

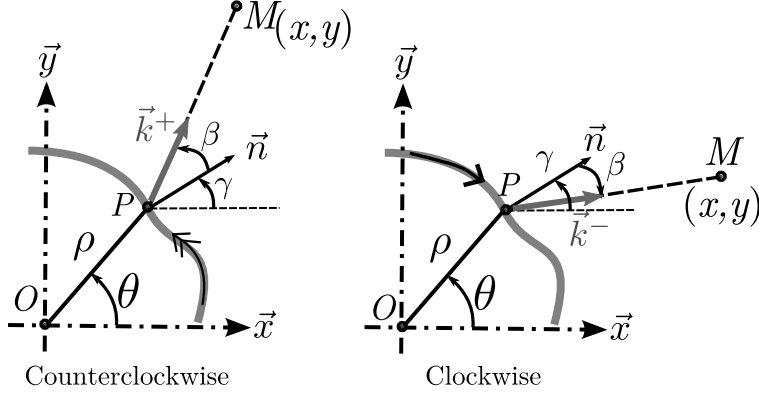


Figure 5: Direction of the radiation \vec{k}^+ and \vec{k}^- for a circumferential wave propagating counterclockwise and clockwise.

107 B Wavefront equation

108 We consider a circumferential guided wave propagating at the phase velocity c_φ and frequency
 109 ω around the shell. This guided wave radiates in the surrounding medium at the angle β .
 110 The radiated wave has the velocity c_0 in the surrounding medium. As the circumferential
 111 waves may propagate in both clockwise (denoted as superscript +) and counterclockwise
 112 (denoted as -) directions along the shell, radiation in the directions \vec{k}^- and \vec{k}^+ will be
 113 considered (fig. 5).

114 The time $t = 0$ is taken when the circumferential wave is at $\theta = 0$ in the shell. At the
 115 time t , a given point M of coordinates (x, y) is reached by a wave radiated in straight line
 116 from the point P of coordinates (ρ, θ) on the shell (Fig. 5). The circumferential wave has
 117 traveled along a distance $s(0, \theta)$ at the celerity c_φ in the shell and the radiated wave has
 118 traveled from P to M at the celerity c_0 .

119 The radiated wavefronts are the set of points M reached at the time t . Considering polar
 120 angles θ in $[0; 2\pi]$, the coordinates of the radiated wavefront $\mathbf{F}^+(t, \theta)$ for a counterclockwise
 121 circumferential wave is (eq. (7)):

$$\mathbf{F}^+(t, \theta) \begin{cases} x(t, \theta) = \rho(\theta) \cos \theta + c_0 \left(t - \frac{s(0, \theta)}{c_\varphi} \right) \cos (\gamma(\theta) + \beta) \\ y(t, \theta) = \rho(\theta) \sin \theta + c_0 \left(t - \frac{s(0, \theta)}{c_\varphi} \right) \sin (\gamma(\theta) + \beta) \end{cases} \quad (7)$$

122 and a similar result for $\mathbf{F}^-(t, \theta)$ radiated by a clockwise circumferential wave (eq. (8)):

$$\mathbf{F}^-(t, \theta) \begin{cases} x(t, \theta) = \rho(\theta) \cos \theta + c_0 \left(t - \frac{s(\theta - 2\pi, 0)}{c_\varphi} \right) \cos(\gamma(\theta) - \beta) \\ y(t, \theta) = \rho(\theta) \sin \theta + c_0 \left(t - \frac{s(\theta - 2\pi, 0)}{c_\varphi} \right) \sin(\gamma(\theta) - \beta) \end{cases} \quad (8)$$

123 In the two formulations (7) and (8), only the physically relevant solutions are considered to
 124 respect causality. These corresponds to the terms describing the propagation in water from
 125 P to M , where the quantity $(t - s/c_\varphi)$ is positive.

126 **C Centers of curvature of the wavefront**

127 Time-reversing the radiated wavefront results in a focal spot at the center of curvature of \mathbf{F}^\pm .
 128 The radius of curvature R_c of these curves is defined from the derivatives of its coordinates
 129 $x(t, \theta)$ and $y(t, \theta)$ with respect to θ

$$R_c(t, \theta) = \frac{(x'^2 + y'^2)^{3/2}}{x'y'' - y'x''}, \quad (9)$$

130 where ' and '' denote the derivatives with respect to θ . The internal normal vector \mathbf{N}_{int} of
 131 the curve is defined for each point $(x(t, \theta), y(t, \theta))$ by equation (10)

$$\mathbf{N}_{\text{int}}(t, \theta) = \frac{1}{\sqrt{x'^2 + y'^2}} \begin{cases} -y' \\ x' \end{cases} \quad (10)$$

132 It is then possible to determine the centers of curvature $\mathbf{C}^+(t, \theta)$ and $\mathbf{C}^-(t, \theta)$ for each
 133 point of the wavefronts $\mathbf{F}^\pm(t, \theta)$ following

$$\mathbf{C}^\pm(t, \theta) = \mathbf{F}^\pm(t, \theta) + R_c(t, \theta)\mathbf{N}_{\text{int}} \quad (11)$$

134 In the case of a circular shell of radius $\rho(\theta) = a$, we have $\gamma(\theta) = \theta$ and $s(0, \theta) = a\theta$. The
 135 above relations simplifies and lead to relations (12).

$$\mathbf{C}_{\text{circle}}^\pm(t, \theta) = \begin{cases} x_c(\theta) = a \frac{c_0}{c_\varphi} \sin(\theta \pm \beta) \\ y_c(\theta) = -a \frac{c_0}{c_\varphi} \cos(\theta \pm \beta) \end{cases} \quad (12)$$

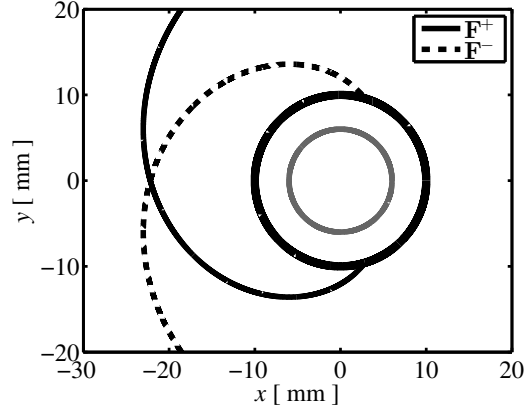


Figure 6: Wavefronts around a circular shell for two circumferential waves (with $a=10$ mm and $c_0/c_\varphi=0.6$). Solid line is for the counterclockwise guided wave and dashed line for the clockwise guided wave. The gray lines are the locus of the centers of curvature of the radiated wavefronts.

136 In this case, $\mathbf{C}_{\text{circle}}^\pm$ does no longer depend on time, implying that it does not depend on
 137 the distance of observation. The centers of curvatures of the wavefronts are located on a
 138 circle of radius $a\frac{c_0}{c_m}$ centered on O . This result is consistent with those of Padilla [11] and
 139 can justify the equation (1) used in [12] and [13]. An example of radiated wavefronts and
 140 their associated centers of curvature is presented in figure 6 in the case of a circular shell.
 141 Due to the symmetry of the configuration, the set of centers of curvature are the same for
 142 both the counterclockwise and the clockwise wavefronts.

143 In the case of an elliptic shell, it is possible to obtain a semi-analytic result, involving
 144 incomplete elliptic integrals, but in the case of a shell of arbitrary cross section, the wavefronts
 145 and their centers of curvature (eqs. (7), (8) and (11)) have to be computed numerically. The
 146 case of an elliptic shell is represented in figure 7. The locus of the centers of curvature
 147 describe a rather complex shape compared to the case of a circular shell. Moreover the locus
 148 corresponding to each wavefront (clockwise and counterclockwise) are different.

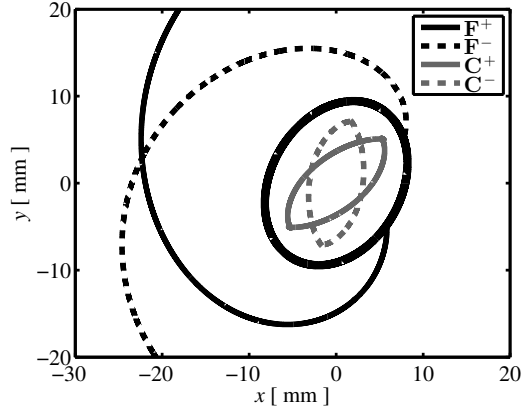


Figure 7: Wavefronts around an elliptic shell for two circumferential waves (with $r_1=10$ mm, $r_2=7.5$ mm and $c_0/c_\varphi=0.6$). Plain line is for the counterclockwise guided wave and dashed line for the clockwise guided wave.

149 **V OBSERVATION OF THE RADIATED WAVEFRONTS BY A TRANS-**
 150 **DUCER ARRAY**

151 In practice, only a small amount of the radiated wavefronts will reach an array of receivers,
 152 arising from a limited part of the shell. Accordingly, the time-reversed received signals will
 153 focus at a reduced number of centers of curvature. Considering the configuration presented
 154 in section II, figure 8 shows the centers of curvature of the part of the wavefronts reaching
 155 the array in the case of a circular shell (a) and of an elliptical shell (b, c). The points
 156 corresponding to the origin of the wavefronts are visible in light gray.

157 The centers of curvature \mathbf{C}^\pm (in gray) are then reduced to a unique point, denoted C_0 ,
 158 which represents the centroid of the centers of curvature for a given wavefront, weighted
 159 by a Hamming window over the elements of the array (this apodization is chosen to attach
 160 greater importance to the central elements, leaving the external elements with a low but
 161 nonzero level). These C_0 points are represented with black points on figure 8. We can notice
 162 that in the case of the elliptical shell the spatial distribution of the centers of curvature \mathbf{C}^\pm
 163 is limited (in the figure, the centers of curvature are often masked by the point representing
 164 their centroid C_0).

165 The expressions of $\mathbf{F}^\pm(t, \theta)$ also depend on time. It is possible to evaluate the phase delay

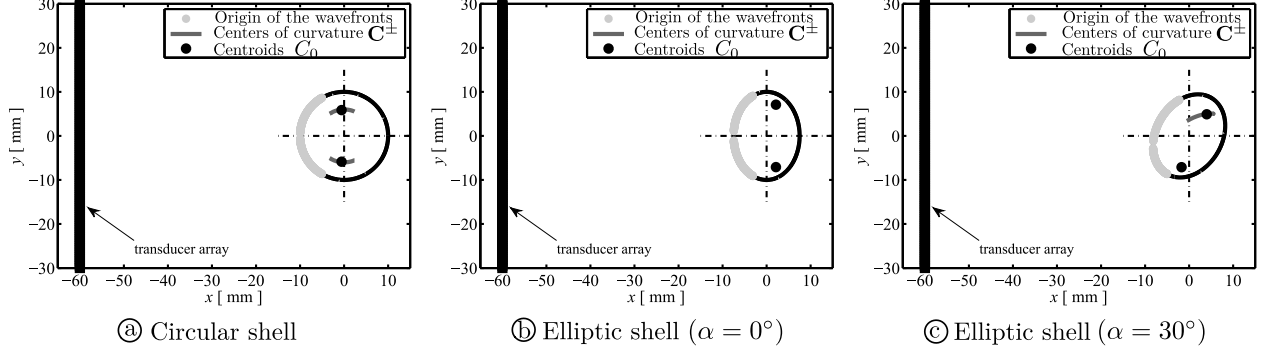


Figure 8: Recording of the wavefronts by a transducer array for a circumferential wave, according to the configuration presented in section II and $c_0/c_\varphi=0.6$.

166 ϕ_i between the signals recorded for each element i of the array. The time-reversal principle
 167 can then be applied using these delays: Assuming a frequency $f_0=1$ MHz and that each
 168 element acts as a point source in plain water with the wavenumber $k_0 = \frac{2\pi f_0}{c_0}$, the field Φ_i
 169 emitted by each element i at the distance r_i in free space is the classical two-dimensional
 170 Green's function in the far field approximation (eq. (13))

$$\Phi_i(r_i, \phi_i) = \frac{e^{i(k_0 r_i + \phi_i)}}{\sqrt{r_i}}. \quad (13)$$

171 Adding the fields Φ_i for each emitter of the array leads to a time-reversed focal spot.
 172 Some examples are presented on figure 9 for the 3 configurations of section II. The position
 173 of the maxima of the focal spots (white star) is very close to the centroids C_0 (white circles)
 174 of the centers of curvature \mathbf{C}^\pm of the wavefronts. This confirms that the time reversal process
 175 focuses on the center of curvature of the wavefronts. This also shows that considering only
 176 the centroids C_0 instead of all the centers of curvature as in fig. 8 is sufficient to evaluate the
 177 position of the focal spots. For the sake of simplicity only the centroids C_0 will be considered
 178 in the following of the paper.

179 In the case of the circular shell, the two centroids C_0 corresponding to the two wavefronts
 180 in opposite directions are symmetric with respect to the horizontal \vec{x} axis. Applying the time
 181 reversal process in this case lead to two focal spots close to the medium axis of the shell, that
 182 is at $x = 0$, referred to as the x_0 -axis in the following. Here, it is important to note that the
 183 method introduced in [12, 13] assumed that time-reversed signals of radiated circumferential
 184 waves focus on the x_0 -axis, which is consistent with the results of figure 9-a. On the contrary,

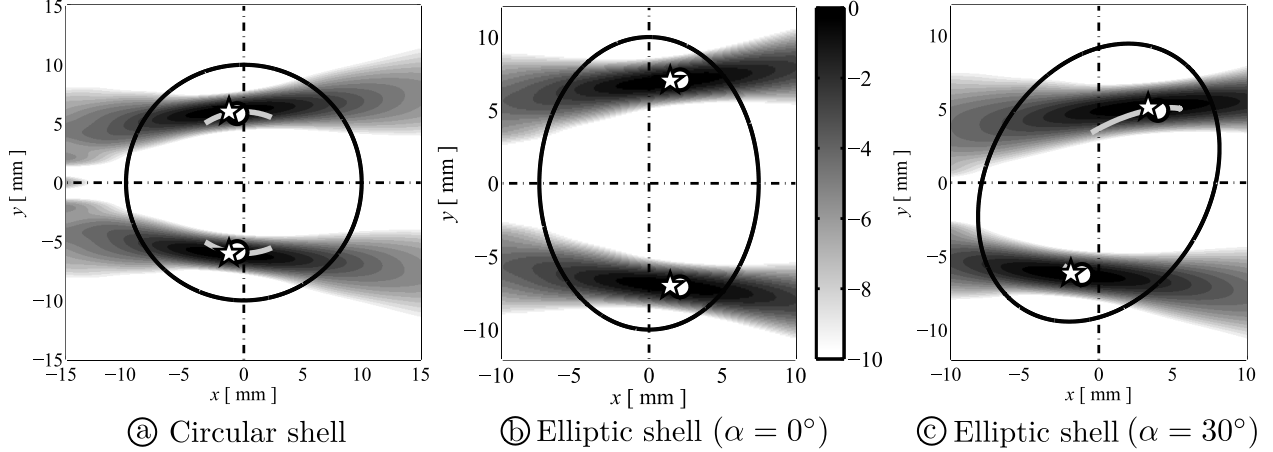


Figure 9: Focal spots obtained by the back-propagation of the wavefronts for a circumferential wave with $c_0/c_\varphi=0.6$, at $f_0=1$ MHz. The white stars indicates the maxima of the focused field, the position of the C^\pm are presented in light gray line and the centroids C_0 are in white circles.

185 for an elliptic shell as in fig. 9-b the two focal spots are no longer on x_0 . Moreover in a general
 186 case of fig. 9-c or with a shell of arbitrary cross section, the focal spots are also no longer
 187 symmetric with respect to the horizontal axis.

188 VI PROPOSED METHOD TO DETERMINE CIRCUMFERENTIAL WAVES 189 PHASE VELOCITIES

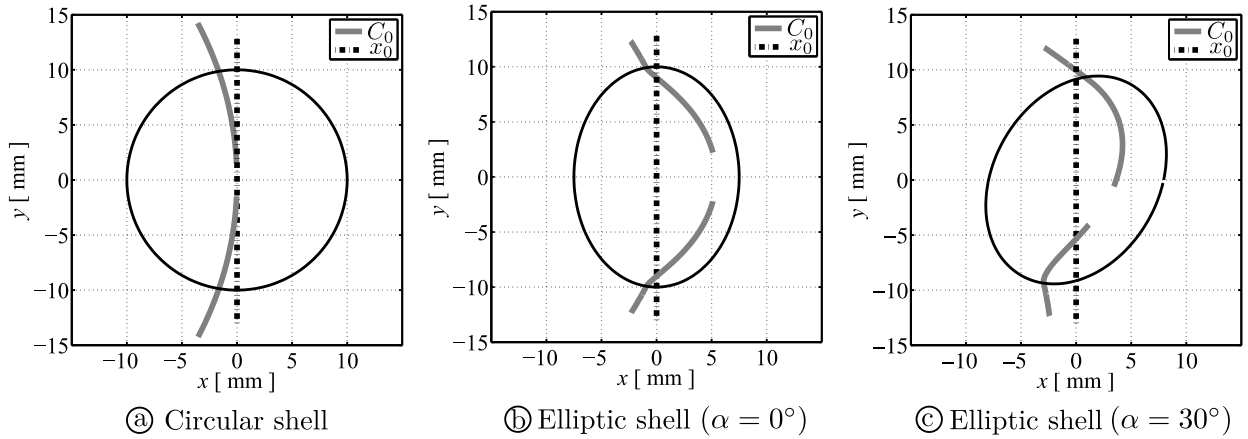


Figure 10: C_0 -curves for various shells with c_φ varying from 1000 to 9000 $\text{m}\cdot\text{s}^{-1}$.

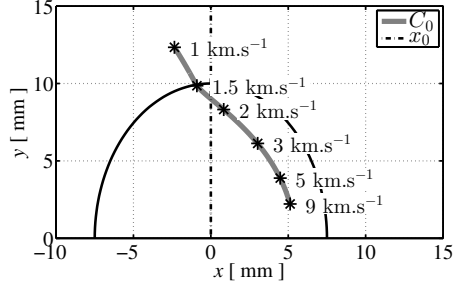


Figure 11: Details of the location of the C_0 points with their relative phase velocities c_φ for the counterclockwise circumferential wave, in the case of an elliptic shell with major axis parallel to the transducer array.

190 The previous section has shown that a given phase velocity c_φ of the circumferential
 191 wave leads to two particular positions of C_0 related to the counterclockwise and clockwise
 192 directions of the wave. Varying the phase velocity provides a set of spatial points C_0 which
 193 constitutes a parametric curve with parameter c_φ referred to as the C_0 -curve (fig. 10) in the
 194 following.

195 Figure 11 presents the details of the phase velocity values on a counterclockwise C_0 -curve.
 196 The points of the curve located outside the shell correspond to c_φ lower than the velocity c_0
 197 in the surrounding fluid. This is similar to the case $d > D$ in eq. (1). Also, when $c_0 = c_\varphi$
 198 (here 1500 m.s^{-1}) the point C_0 is located exactly on the surface of the shell. The part of
 199 the C_0 -curve outside the shell can account for generalized Stoneley waves and Franz waves
 200 (creeping waves).

201 Figure 11 shows that the points of the C_0 -curve towards the center of the object, corre-
 202 sponding to the highest values of c_φ , are closer one to the others than the points corresponding
 203 to the lowest values of c_φ . In other words, the distribution of c_φ along the curve is denser
 204 as the velocity increases. This is illustrated, for example, by the 'short' distance between
 205 the points corresponding to $c_\varphi = 5$ and 9 km.s^{-1} , compared to the relatively 'long' distance
 206 between $c_\varphi = 2$ and 3 km.s^{-1} .

207 The principle of the proposed method to measure phase velocities of circumferential waves
 208 is to use a predefined C_0 -curve. Such a curve can be calculated knowing only the position
 209 and external geometrical shape of the shell. Note that there is no hypothesis made over the

210 thickness of the shell nor on the material properties: only the propagation of a circumferential
211 wave with a given phase velocity is assumed. The proposed method is outlined below:

- 212 1. Calculate with eq. (11) the C_0 -curve corresponding to the measured object (position,
213 external geometry and range of expected phase velocities), given the relative positions
214 and size of the object and the transducer ;
- 215 2. Excite circumferential waves in the shell and record the waves radiated in the sur-
216 rounding medium with a transducer array;
- 217 3. Fourier-transform the recorded signals;
- 218 4. In cases where time-domain signals of several circumferential modes overlap, the DORT
219 method can be used to separate the contribution of each mode and eliminate the non
220 significant contributions along with noise;
- 221 5. Calculate, for each frequency, the amplitude of the back-propagated wavefield along
222 the predefined C_0 -curve. The phase velocity of the circumferential wave (or of the
223 mode selected at step #4 in cases where several guided modes exist) corresponds to
224 the point of the C_0 -curve where the wavefield is maximum, that is, in practice, at the
225 intersection between the C_0 -curve and a focal spot.

226 The method involving the use of eq. (1) and (2) can also be used but only in the case
227 (a) and (b) of figure 10, where the shell is symmetric relative to the x -axis. In this case it is
228 sufficient to calculate the back-propagated wavefield on the x_0 -axis, measure the distance d
229 between the two focal spots and apply the analytic equations to recover the phase velocities.
230 This much simpler method will be referred as the “ x_0 method” in the following. In the case
231 of a circular shell (fig 10-a), the C_0 curve is very close to the medium axis of the shell x_0 . In
232 this case the use of the x_0 method may be sufficient to compute the dispersion curve. In the
233 case of the elliptic shell with a major axis parallel to the transducer array (fig 10-b), as the
234 C_0 curve is rather different from the x_0 curve, the x_0 method may still be practicable but
235 will provide different results. In the general case of shell with arbitrary cross section, the x_0
236 method is not practicable.

237 The heterogeneous distribution of c_φ values along the C_0 -curve discussed above has im-
238 portant consequences as a better resolution will be obtained for the estimations of low c_φ
239 than of high c_φ . In particular in the non symmetric case (here in fig 10-c) the C_0 curve in
240 the lower part corresponding to the centroids for the clockwise circumferential wave is quite
241 short and all points are close one to another; it will be more difficult to distinguish different
242 phase velocities as the focal spots will cover a large amount of these points. On the contrary
243 the upper part presents points spreaded in space and then provide a better resolution on c_φ .

244 VII NUMERICAL VALIDATION

245 Numerical simulations have been used to validate our approach. Simulations were performed
246 with a two-dimensional Time-Domain Finite Difference (FDTD) code SIMSONIC [21, 24].
247 The configuration of the simulations is the same as described in section II.

248 In order to perform the Singular Value Decomposition (SVD) needed by the DORT
249 method [14, 13, 25], the response function of the transducer array was obtained with emissions
250 from 32 elements evenly spaced along the array. The reception is performed with all the 128
251 elements. The source signal emitted by each element of the array is a Ricker wavelet (or
252 Mexican hat) with a central frequency $f_0=1$ MHz. The spatial step of the simulation grid
253 is $h=0.025$ mm and a preliminary study on homogeneous mediums has shown the numerical
254 dispersion to be much less than 1% in that case.

255 The dispersion curves of guided waves modes measured with the proposed method are
256 compared to reference curves calculated for a plane plate loaded with water on one side and
257 free on the other side [26].

258 Figure 12 presents an example of snapshot recorded during the simulations. The presence
259 of several modes of circumferential waves propagating around the shell is visible, along with
260 the wavefronts radiated in water. The shape of these simulated wavefronts is similar to the
261 geometrical shapes computed with equations (7) and (8).

262 As there are several modes of propagation for the circumferential waves, each of them
263 radiating in the fluid, several radiated wavefronts interfere. The use of the DORT method
264 on the recorded signals at the receivers will allow to separate the major contributions of
265 the radiated field. This is done by considering only a few high singular vectors of the time

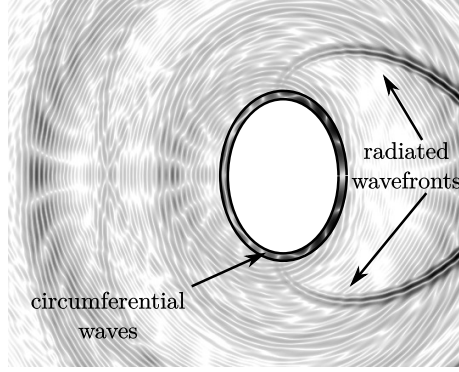


Figure 12: Snapshot of the simulation of circumferential waves around an elliptic shell and radiating in the surrounding medium.

266 reversal operator, discarding the others. Doing so eliminates all the components with a low
 267 signal-to-noise ratio. The highest singular vectors are used to calculate the retro-propagated
 268 wavefield on the C_0 -curve calculated as indicated in the previous sections. When possible
 269 (case of a circular shell or an elliptic shell with major axis parallel to the array), the x_0
 270 method will also be performed as a way of comparison. As these two cases are symmetric
 271 with respect to the horizontal axis, only the counterclockwise wave i.e. the upper part of
 272 the shell will be considered.

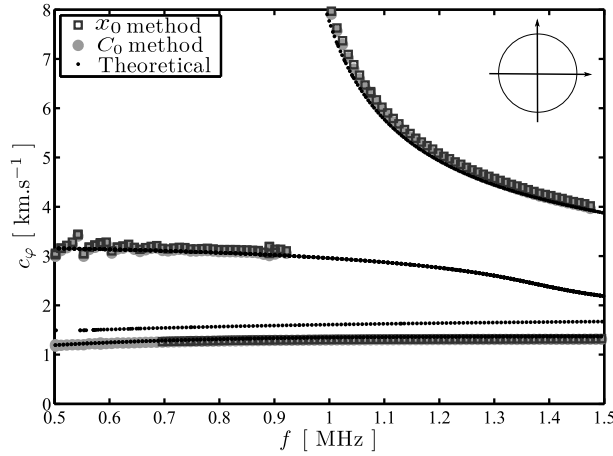


Figure 13: Dispersion curves for a circular shell of thickness $e=1$ mm. The squares represents the results obtained from the x_0 method (eq. (1)), and the gray rounds represents the results obtained with the C_0 method.

273 The results obtained on a circular shell are presented on figure 13. The classical x_0 method

274 and the C_0 method provide almost the same results, as expected from fig. 10-a where the
 275 C_0 -curve is very close to the x_0 -axis. The agreement with the theoretical dispersion curves is
 276 very good and allows to recover the branches identified as the S0 and the A1 Lamb modes.
 277 The lower branch with a velocity close to 1000 m.s^{-1} corresponds to the generalized Stoneley
 278 wave at the interface with the shell. These excellent results on the circular shell validate our
 279 approach and approximations, along with the simulations tools used. In the following, only
 280 the external shape of the shell is changed.

281 Figure 14 presents the results for an elliptic shell with its major axis parallel to the
 282 transducer array. Significant discrepancies are found between the results of the x_0 - and C_0 -
 283 methods, especially for the higher velocities (A1 mode). The results from the C_0 method
 284 are closer to the reference theoretical curves than those of the x_0 method. They are within
 285 10% of the reference values.

286 For an elliptic shell with an arbitrary inclination the x_0 method is not available (Fig. 15).
 287 Due to the non-symmetry of the shell related to the horizontal axis, the branches of the
 288 dispersion curves may be evaluated considering the counterclockwise circumferential waves
 289 (upper part of the shell) or the clockwise waves (lower part), leading to different results.
 290 Using counterclockwise waves, the agreement with the theoretical modes is excellent while
 291 it is less good using clockwise waves This may be partly explained considering the positions
 292 of the C_0 points on fig. 10-c, where the points corresponding to the upper part are more
 293 spreaded in space leading to a better resolution of the method.

294 VIII DISCUSSION AND CONCLUSION

295 The paper presented a method to estimate the phase velocity of the circumferential waves
 296 around thin shells in a non contact way. It applies to shells of any shape, provided the
 297 external geometry is known, along with the position and size of the transducer array. As
 298 the computation of the C_0 curves only depend on the external geometry of the shell, this
 299 method may also be suitable to study shells with varying thickness. In the same way, the
 300 mechanical properties of the shell may vary along the shell. In these cases the estimation
 301 of the phase velocities is only related to the part of the shell where the wavefronts recorded
 302 by the receivers were emitted. The computation of $\mathbf{F}^\pm(t, \theta)$ allows determining the origins

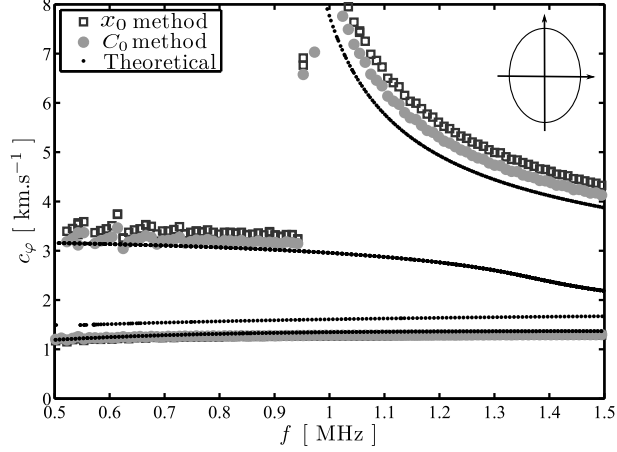


Figure 14: Dispersion curves for an elliptic shell ($e=1$ mm) which major axis parallel to the transducer array. The squares represents the results obtained from the x_0 method (eq. (2)), and the gray circles represents the results obtained with the C_0 method.

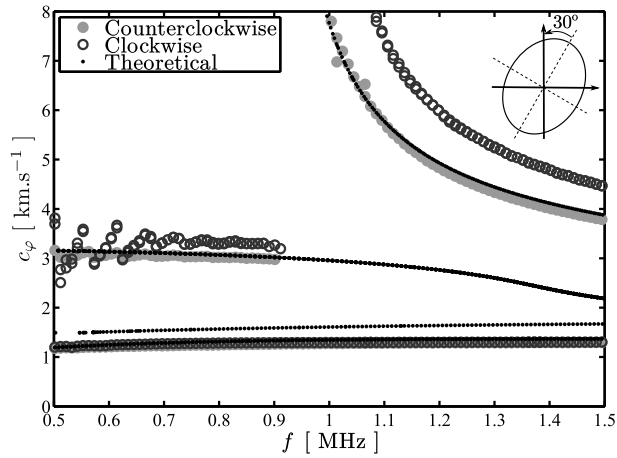


Figure 15: Dispersion curves for an elliptic shell ($e=1$ mm) with an inclination of 30° .

303 of the wavefronts reaching the receivers (see for example fig. 8) and thus the portion of the
 304 shell investigated.

305 However there are a few limitations to the technique. First the circumferential waves
 306 have to be generated in the shell by the incident wave from the transducer. Some modes of
 307 circumferential may not be excited and thus their associated branches in the dispersion curve
 308 will not be estimated. Second, the circumferential waves also have to propagate around the
 309 shell and radiate in the surrounding medium. This may induce an important attenuation: if
 310 the attenuation is too important the circumferential wave will not be able to circle around

311 the shell and to radiate toward the receiver.

312 When considering a geometry of shell, it is important to look at the shape of the C_0 -curve,
313 and in particular at the distribution of the velocities along this curve. In practice, if the C_0
314 points corresponding to different phase velocities are too close, the focal spots of the time
315 reversal process will not be able to distinguish between them. Therefore, the orientation of
316 the shell relative to the position of the array is important : an orientation which leads to the
317 C_0 points the more spreaded in space as possible is preferred. In any cases, the resolution
318 for lower velocities is much better than for the velocities greater than $3\text{-}4\text{ km.s}^{-1}$. Another
319 limitation is that all the dimensions and the relative positions have to be known precisely, as
320 a small error in the position of the C_0 -curve ($<1\text{ mm}$) may lead to a difference greater than
321 500 m.s^{-1} .

322 For the non-circular cases, e.g. fig 14 and 15, the maximal error with the reference value
323 is about 10% for high velocities. As the results obtained with the circular shell are excellent,
324 this error cannot come from the simulation tool used, nor from the fact that the curvature
325 of the shell is neglected in the reference value (Lamb waves in a plane plate). The origin of
326 the error is still not fully explained and has to be investigated further.

327 The method presented here can be useful in medical applications, for example to evaluate
328 the mechanical properties of bones like femoral neck *in vitro* or *in vivo* where the cortical
329 (compact) part of the bone can be considered as a shell of varying geometry, thickness and
330 properties, immersed in a fluid. Some industrial application may also be found as the method
331 is suitable for a non contact inspection and evaluation of any tubular component, like pipes
332 for instance.

333 ACKNOWLEDGEMENTS

334 The authors wish to thank Dr Maryline Talmant and Dr Pierre Nauleau for her helpful
335 comments and discussions. The authors are grateful for the financial support of UPMC in
336 the framework of the program Emergence 2009 (Post-Doctoral Fellowship M. Chekroun).

337 **References**

- 338 [1] R. D. Doolittle, H. Uberall, and P. Ugincius. Sound scattering by elastic cylinders. *J.*
339 *Acoust. Soc. Am.*, 43(1):1–14, 1968.
- 340 [2] G. V. Frisk, J.W. Dickey, and H. Uberall. Surface wave modes on elastic cylinders. *J.*
341 *Acoust. Soc. Am.*, 58(5):996–1008, 1975.
- 342 [3] G. V. Frisk and H. Uberall. Creeping waves and lateral waves in acoustic scattering by
343 large elastic cylinders. *J. Acoust. Soc. Am.*, 59(1):46–54, 1976.
- 344 [4] J.B. Keller. Geometrical theory of diffraction. *J. Opt. Soc. Am.*, 52(2):116–130, 1962.
- 345 [5] Philip L. Marston. GTD for backscattering from elastic spheres and cylinders in water
346 and the coupling of surface elastic waves with the acoustic field. *J. Acoust. Soc. Am.*,
347 83(1):25–37, 1988.
- 348 [6] W. G. Neubauer. Pulsed Circumferential Waves on Aluminum Cylinders in Water. *J.*
349 *Acoust. Soc. Am.*, 45(5):1134–1144, 1969.
- 350 [7] N. Gespa. *La diffusion acoustique par des cibles élastiques de forme géométrique simple:*
351 *Theorie et Experiences.* Centre de Documentation de l’Armement, Paris, 639 pages,
352 1987.
- 353 [8] Z. Wu, G. Zhou, and S. Feng. Visualization of the sound scattering by a cylinder. *Acta*
354 *Acustica*, 18:81–90, 1993.
- 355 [9] E. Heyman and L. B. Felsen. Traveling wave and SEM representations for transient
356 scattering by a circular cylinder. *J. Acoust. Soc. Am.*, 79(2):230–238, 1986.
- 357 [10] W. Hassan and P. B. Nagy. Circumferential creeping waves around a fluid-filled cylin-
358 drical cavity in an elastic medium. *J. Acoust. Soc. Am.*, 101(5):2496–2503, 1997.
- 359 [11] F. Padilla, B. Poirée, M. Talmant, and G. Quentin. The wave bivector formalism
360 associated with circumferential leaky waves. *J. Acoust. Soc. Am.*, 108(1):25–30, 2000.

- 361 [12] J.L. Thomas, P. Roux, and M. Fink. Inverse Scattering with an Acoustic Time-Reversal
362 Mirror. *Phys. Rev. Lett.*, 72:637–640, 1994.
- 363 [13] C. Prada and M. Fink. Separation of interfering acoustic scattered signals using the
364 invariants of the time-reversal operator. Application to Lamb waves characterisation. *J.*
365 *Acoust. Soc. Am.*, 104(2):801–807, 1998.
- 366 [14] C. Prada and M. Fink. Eigenmodes of the time reversal operator: A solution to selective
367 focusing in multiple-target media. *Wave Motion*, 20(2):151 – 163, 1994.
- 368 [15] P. Nauleau, E. Cochard, J.-G. Minonzio, Q. Grimal, P. Laugier, and C. Prada. Char-
369 acterization of circumferential guided waves in a cylindrical cortical bone-mimicking
370 phantom. *J. Acoust. Soc. Am.*, 131(4):EL289–EL294, 2012.
- 371 [16] P. Nauleau, Q. Grimal, J.-G. Minonzio, P. Laugier, and C. Prada. Circumferential
372 guided wave measurements of a cylindrical fluid-filled bone-mimicking phantom. *J.*
373 *Acoust. Soc. Am.*, 135(2):994–1001, 2014.
- 374 [17] M. Chekroun, Q. Grimal, E Cochard, J.-G. Minonzio, C. Prada, and P Laugier. Mesure
375 des courbes de dispersion des ondes guidées circonférentielles dans une coque elliptique
376 par retournement temporel. (Measurement of circumferential guided waves dispersion
377 curves in an elliptic shell using time reversal). In *proceedings of the 20th Congrès Français*
378 *de Mécanique, Besançon, France*, august 2011. <http://hdl.handle.net/2042/46432>
379 (date last viewed 3/23/15).
- 380 [18] G.S. Sammelmann, D. H. Trivett, and R. H. Hackman. The acoustic scattering by a
381 submerged, spherical shell. I: The bifurcation of the dispersion curve for the spherical
382 antisymmetric Lamb wave. *J. Acoust. Soc. Am.*, 85(1):114–124, 1989.
- 383 [19] M. Talmant, J. M. Conoir, and J.-L. Rousselot. High frequency scattering by shells.
384 *Acta Acustica*, 3:509–515, 1995.
- 385 [20] G. Maze, F. Leon, J. Ripoche, and H. Uberall. Repulsion phenomena in the phase-
386 velocity dispersion curves of circumferential waves on elastic cylindrical shells. *J. Acoust.*
387 *Soc. Am.*, 105(3):1695–1701, 1999.

- 388 [21] E. Bossy, M. Talmant, and P. Laugier. Three-dimensional simulations of ultrasonic
389 axial transmission velocity measurement on cortical bone models. *J. Acoust. Soc. Am.*,
390 115:2314–2324, 2004.
- 391 [22] K. L. Williams and P. L. Marston. Backscattering from an elastic sphere: Sommerfeld–
392 Watson transformation and experimental confirmation. *J. Acoust. Soc. Am.*,
393 78(3):1093–1102, 1985.
- 394 [23] M. Fink. Time-Reversal of ultrasonic fields–Part I : Basic principles. *IEEE T. Ultrason.*
395 *Ferr.*, 39(5):555–566, 1992.
- 396 [24] Emmanuel Bossy. Simsonic software suite for the simulation of ultrasound propagation.
397 <http://www.simsonic.fr/> (date last viewed 3/23/15), 2012.
- 398 [25] J.-G. Minonzio, C. Prada, D. Chambers, D. Clorennec, and M. Fink. Characterization
399 of subwavelength elastic cylinders with the decomposition of the time-reversal operator:
400 Theory and experiment. *J. Acoust. Soc. Am.*, 117(2):789–798, 2005.
- 401 [26] B Pavlakovic and M Lowe. Disperse software, v. 2.0. 16. *Mechanical Engineering,*
402 *Imperial College, London*, 2005.

403 **List of Figures**

404 1 Geometrical construction of the radiated wavefront by a circumferential wave
405 around a circular cylinder (adapted from ref. [6]). 3

406 2 General configuration of the setup used to evaluate the dispersion curves of
407 the circumferential guided waves around a thin cylindrical shell. 5

408 3 Principle of the generation and radiation of circumferential waves around a
409 thin circular cylinder. 6

410 4 Notations used to describe the radiation of a circumferential wave around a
411 shell of arbitrary cross section. 7

412 5 Direction of the radiation \vec{k}^+ and \vec{k}^- for a circumferential wave propagating
413 counterclockwise and clockwise. 8

414 6 Wavefronts around a circular shell for two circumferential waves (with $a=10$ mm
415 and $c_0/c_\varphi=0.6$). Solid line is for the counterclockwise guided wave and dashed
416 line for the clockwise guided wave. The gray lines are the locus of the centers
417 of curvature of the radiated wavefronts. 10

418 7 Wavefronts around an elliptic shell for two circumferential waves (with $r_1=10$ mm,
419 $r_2=7.5$ mm and $c_0/c_\varphi=0.6$). Plain line is for the counterclockwise guided wave
420 and dashed line for the clockwise guided wave. 11

421 8 Recording of the wavefronts by a transducer array for a circumferential wave,
422 according to the configuration presented in section II and $c_0/c_\varphi=0.6$ 12

423 9 Focal spots obtained by the back-propagation of the wavefronts for a circum-
424 ferential wave with $c_0/c_\varphi=0.6$, at $f_0=1$ MHz. The white stars indicates the
425 maxima of the focused field, , the position of the \mathbf{C}^\pm are presented in light
426 gray line and the centroids C_0 are in white circles. 13

427 10 C_0 -curves for various shells with c_φ varying from 1000 to 9000 m.s⁻¹. 13

428 11 Details of the location of the C_0 points with their relative phase velocities c_φ
429 for the counterclockwise circumferential wave, in the case of an elliptic shell
430 with major axis parallel to the transducer array. 14

431	12	Snapshot of the simulation of circumferential waves around an elliptic shell and radiating in the surrounding medium.	17
432			
433	13	Dispersion curves for a circular shell of thickness $e=1$ mm. The squares represents the results obtained from the x_0 method (eq. (1)), and the gray rounds represents the results obtained with the C_0 method.	17
434			
435			
436	14	Dispersion curves for an elliptic shell ($e=1$ mm) which major axis parallel to the transducer array. The squares represents the results obtained from the x_0 method (eq. (2)), and the gray circles represents the results obtained with the C_0 method.	19
437			
438			
439			
440	15	Dispersion curves for an elliptic shell ($e=1$ mm) with an inclination of 30°	19